Polyhedron 73 (2014) 37–44

Contents lists available at ScienceDirect

Polyhedron

journal homepage: www.elsevier.com/locate/poly

Copper catalyzed oxidation of amino acids

Szabina Góger [a], József S. Pap [a], Dóra Bogáth [a], A. Jalila Simaan [b], Gábor Speier [a], Michel Giorgi [c], József Kaizer [a,*]

[a] Department of Chemistry, University of Pannonia, H-8200 Veszprém, Hungary
[b] Aix Marseille Université, CNRS, Centrale Marseille, iSm2 UMR 7313, 13397 Marseille, France
[c] Aix-Marseille Université, FR1739, Spectropole, Campus St. Jérôme, Avenue Escadrille Normandie-Niemen, 13397 Marseille cedex 20, France

ARTICLE INFO

Article history:
Received 27 November 2013
Accepted 5 February 2014
Available online 18 February 2014

Keywords:
Biomimetic oxidation
Oxidase activity
Kinetic studies
Amino acids
Copper(II)

ABSTRACT

Copper(II) chloride and novel *bis*(1-amino(cyclo)alkane-1-carboxylato-κ^2N,O)copper(II) complexes as catalysts were studied in relation with enzymatic oxidation of amino acids. The oxidation of aminophosphonate derivative: (1-amino-1-methyl)ethylphosphonic acid was also investigated. Two *bis*(1-aminocycloalkane-1-carboxylato-κ^2N,O)copper(II) complexes were structurally characterized. Surprisingly, while the 1-aminocyclobutane-1-carboxylate complex has square planar (*SP*-4) copper(II) center with *trans*-orientated ligands, the 1-aminocyclohexane-1-carboxylate complex has μ-carboxylato dimeric structure with square pyramidal (*SPY*-5) sites, one with *cis*- and one with *trans*-orientated ligands. Redox behavior of the *bis*(1-amino(cyclo)alkane-1-carboxylato-κ^2N,O)copper(II) complexes was also investigated. Catalytic oxidations were carried out in alkaline DMF-water mixtures using H_2O_2 as oxidant and the complexes as catalysts. The observed potentials for the irreversible current peaks associated with the Cu(II) to Cu(I) reduction and the rates of the amino acid oxidations show inverse trend. This suggests that the Cu(II)/Cu(I) redox cycling due to the presence of H_2O_2 plays important role in the peroxide/copper activation that in turn provides the observed products.

1. Introduction

The oxidative degradation of organic substances such as amino acids under mild conditions is of great interest for industrial and synthetic processes both from an economical and environmental point of view. Amino acids may form potentially harmful disinfection byproducts during the conventional treatment of water and wastewater [1,2]. Removal of these parent compounds by the use of the environmental-friendly oxidant, ferrate(VI) was assessed by studying the kinetics of the oxidation of glycine [3]. Previously, kinetics and mechanism of oxidation of neutral L-amino acids by sodium *N*-chloro-*p*-toluene sulfonamide in acid [4,5] and alkaline medium [6] have been reported.

Metal ion-catalyzed oxidations (MCO) of amino acids were also performed by researchers to mimic the deamination of bioactive molecules catalyzed by enzymes. The first example of a biomimetic mononuclear iron complex, ([Fe^{III}(Salen)Cl] (Salen = *N*,*N*′-bis (salicylidene)-ethylenediaminato) was described, that highly selectively and efficiently catalyzes the oxidation of a series of acyclic and cyclic amino acids to ethylene or the corresponding carbonyl compounds [7,8] (Scheme 1), mimicking the action of the non-heme iron enzyme 1-aminocyclopropane-1-carboxylic acid oxidase (ACCO) [9]. Kinetics and mechanism of the oxidation of α-amino acids by peroxomonosulphate (PMS) in acetic acid/sodium acetate buffered [10–16], and alkaline medium were also reported [17].

Besides enzymatic reactions, the oxidation of amino acids or amino acid residues in living organisms may occur either by reactive oxygen species (ROS) [18] or as a MCO process [19]. ROS-indicated oxidation reactions of amino acids and the products formed are well described, and understood [20]. Much less is known this far about MCO, however metal-based oxidants have far greater potential [21]. MCO gives rise to highly reactive intermediates such as hydroxyl radicals, which lead to damage in bio-molecules such as proteins that are implicated in aging and the pathogenesis of neurodegenerative diseases, including Alzheimer's disease [22,23].

Here we describe a new copper(II)-catalyzed (Table 1) system for a series of acyclic (α-amino-isobityric acid (AIBH), D,L-alanine (D,L-ALAH)) and cyclic amino acids (1-aminocyclopropane-1-carboxylic acid (ACCH), 1-amino-1-cyclobutanecarboxylic acid (ACBCH), 1-aminocyclopentanecarboxylic acid (ACPCH), and 1-aminocyclohexanecarboxylic acid (ACHCH)), and α-aminophosphonic acid ((1-amino-1-methyl)ethylphosphonic acid (AMEP))

* Corresponding author. Tel.: +36 88 624 720; fax: +36 88 624 469.
E-mail address: kaizer@almos.vein.hu (J. Kaizer).

http://dx.doi.org/10.1016/j.poly.2014.02.007
0277-5387/

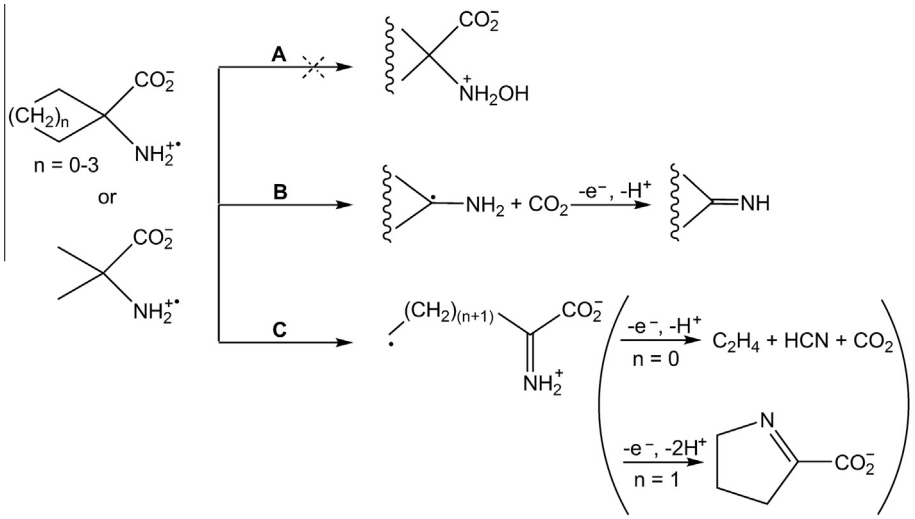

Scheme 1. Pathways leading to different products by ACCO.

Table 1
Summary of the isolated complexes.

Amino acid (AA)	$[Cu^{II}_n(AA)_{2n}]\cdot mH_2O$
ACBC	**1** ($n = 1$, $m = 0$)
ACPC	**2** ($n = 1$, $m = 1$)
ACHC	**3** ($n = 2$, $m = 2$)[a]
AIB	**4** ($n = 1$, $m = 0$)
D,L-ALA	**5** ($n = 1$, $m = 1$)

[a] one water molecule is coordinated.

as surrogates for the corresponding α-aminocarboxylic acids (Scheme 2, Table 1).

2. Experimental

2.1. Materials

Solvents used for the reactions were purified by literature methods [24] and stored under argon. All other chemicals were commercial products and were used as received without further purification. The $Cu(ClO_4)_2\cdot 6H_2O$ and the amino acid substrates and AMEPH were purchased from commercial sources.

2.2. Analytical and physical measurements

Infrared spectra were recorded on an Avatar 330 FT-IR Thermo Nicolet instrument using samples mulled in in KBr pellets. UV–Vis spectra were recorded on a Cary 60 spectrophotometer equipped with a fiber-optic probe with 1 cm pathlength. Microanalyses were done by the Microanalytical Service of the University of Pannonia. Cyclic voltammograms (CV) were taken on a VoltaLab 10 potentiostat with VoltaMaster 4 software for data process. The electrodes were as follows: glassy carbon (working), Pt (auxiliary), and Ag/AgCl in 3 M KCl (reference). The potentials were referenced *vs.* the ferrocenium ferrocene redox couple (+416 mV in methanol in our setup). The crystal evaluations and intensity data collections were performed on a Bruker-Nonius Kappa CCD single-crystal diffractometer (**1**, **3**) using Mo Kα radiation ($\lambda = 0.71070$ Å) at

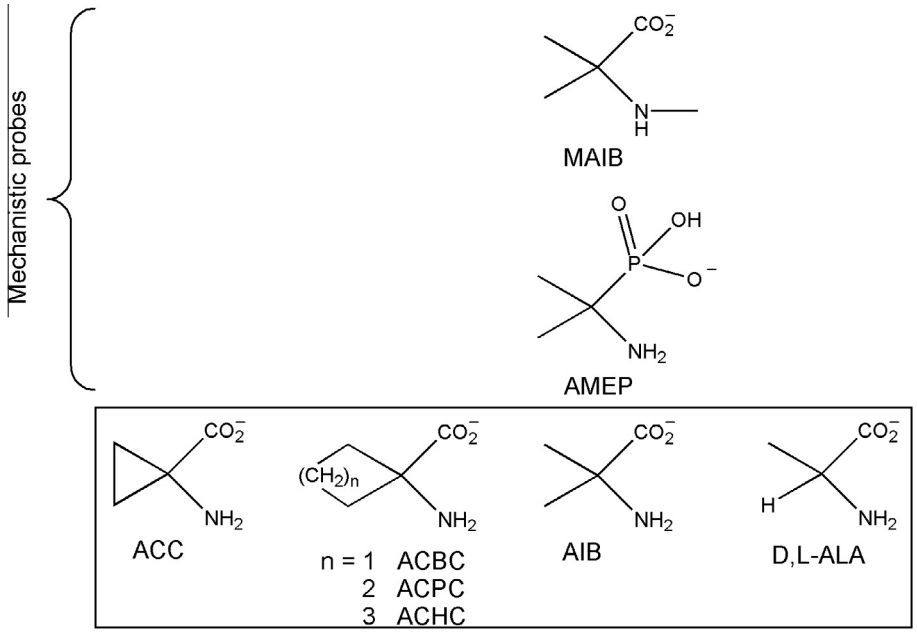

Scheme 2. Structures and abbreviated names of the substrates used in this study.

296, 293, and 203 K, respectively. Crystallographic data and details of the structure determination are given in Table 2, whereas selected bond lengths and angles are listed in Tables 3–6. SHELX-97 [25] was used for structure solution and full matrix least squares refinement on F^2. CIF files are available in the CCDC database: CCDC 941371–941372 (**1**, **3**). GC measurements were performed on a HP 5890 gas chromatograph equipped with a 30 m Supelcowax coloumn.

2.3. Synthesis of $[Cu^{II}(ACBC)_2]$ (**1**)

A 5 mL aqueous solution of ACBCH (0.69 g, 6 mmol) was mixed with $CuCl_2{\cdot}2H_2O$ (0.51 g, 3 mmol) in 15 mL CH_3OH and triethylamine (0.84 mL, 6 mmol) was added slowly to the mixture. Formation of a purple-blue crystalline precipitate was observed following the disappearance of a transient lilac colour. Yield: 0.56 g (64%). *Anal.* Calc. for $C_{10}H_{16}CuN_2O_4$: C, 41.16; H, 5.53; N, 9.60. Found: C, 41.4; H, 5.6; N, 9.8%. FT-IR bands (KBr pellet, cm^{-1}) 3285 (m), 3238 (m), 3126 (w), 2974 (w), 2950 (w), 2868 (w), 1619 (vs), 1391 (s), 1272 (s), 1158 (s), 1070 (m), 751 (w), 690 (w), 571 (w). UV–Vis (CH_3OH/water) [λ_{max}, nm ($\log\varepsilon$)] 243 (4.00), 611 (2.06). Crystals suitable for X-ray structural determination were obtained from CH_3OH–water solvent mixture.

Complexes **2**–**5** were synthesized analogously to **1**.

2.4. Synthesis of $[Cu^{II}(ACPC)_2]{\cdot}H_2O$ (**2**)

Yield: 0.71 g (74%). *Anal.* Calc. for $C_{12}H_{22}CuN_2O_5$: C, 42.66; H, 6.56; N, 8.29. Found: C, 42.7; H, 6.6; N, 8.4%. FT-IR bands (KBr pellet, cm^{-1}) 3446 (m), 3284 (m), 3248 (m), 2959 (w), 2870 (w), 1625 (vs), 1583 (s), 1374 (s), 1326 (w), 1186 (m), 1148 (m), 821 (m), 645 (w), 596 (w). UV–Vis (CH_3OH) [λ_{max}, nm ($\log\varepsilon$)] 245 (3.89), 594 (1.94).

2.5. Synthesis of $[Cu^{II}_2(ACHC)_4(H_2O)]{\cdot}H_2O$ (**3**)

Yield: 0.65 g (62%). *Anal.* Calc. for $C_{28}H_{52}Cu_2N_4O_{10}$: C, 45.95; H, 7.16; N, 7.66. Found: C, 46.3; H, 7.2; N, 7.8%. FT-IR bands (KBr pellet, cm^{-1}) 3441 (m), 3320 (m), 3250 (m), 3147 (w), 2929 (s), 2859 (s), 1612 (vs), 1603 (s), 1453 (m), 1369 (s), 1343 (s), 1175 (m), 1098 (m), 983 (w), 814 (m), 757 (w), 670 (w), 561 (w). UV–Vis (CH_3OH) [λ_{max}, nm ($\log\varepsilon$)] 245 (3.84), 595 (1.85). Crystals suitable for X-ray structural determination were obtained from CH_3OH–water solvent mixture.

Table 2
Crystal structure details for **1** and **3**.

Compound reference	**1**	**3**
Chemical formula	$C_5H_8Cu_{0.5}NO_2$	$C_{28}H_{52}Cu_2N_4O_{10}$
Formula mass	145.89	731.82
Crystal system	monoclinic	monoclinic
a (Å)	10.381(1)	10.733(1)
b (Å)	5.1906(5)	13.629(1)
c (Å)	9.912(1)	22.776(3)
α (°)	90	90
β (°)	90.345	100.41(5)
γ (°)	90	90
Unit cell volume (Å^3)	534.08(9)	3276.8(6)
T (K)	293(2)	293(2)
Space group	$P2_1/c$	$P2_1/c$
Number of formula units per unit cell, Z	4	4
Radiation type	Mo Kα	Mo Kα
Absorption coefficient (μ/mm^{-1})		
No. of reflections measured	5465	38240
No. of independent reflections	1293	7987
R_{int}	0.1051	0.081
Final R_1 values ($I > 2\sigma(I)$)	0.0587	0.0524
Final wR values ($I > 2\sigma(I)$)	0.1369	0.1291
Final R_1 values (all data)	0.1379	0.1185
Goodness of fit (GOF)	0.971	1.028
CCDC number	941371	941372

Table 3
Selected bond lengths (Å) for **1** and **3**.

1			
Cu1–N1	1.987(6)	Cu1–O1	1.968(5)
3			
Cu1–N1	1.984(3)	Cu2–N3	1.978(2)
Cu1–N2	1.988(3)	Cu2–N4	1.977(3)
Cu1–O1	1.959(2)	Cu2–O1	2.537(2)
Cu1–O3	1.942(3)	Cu2–O6	1.944(2)
Cu1–O5	2.349(2)	Cu2–O8	1.927(2)
τ(Cu1)	0.34	τ(Cu1)	0.11

Table 4
Selected bond angles (°) for **1** and **3**.

1			
N1–Cu1–O1	83.7(2)	N1–Cu1–O1	96.3(2)
N1–Cu1–N1	180.0(3)	C3–C2–C5	87.1(6)
3			
N1–Cu1–N2	175.2(1)	N3–Cu2–O1	88.42(9)
N1–Cu1–O1	83.4(1)	N3–Cu2–O6	85.0(1)
N1–Cu1–O5	91.8(1)	N3–Cu2–O8	178.2(1)
N2–Cu1–O3	83.8(1)	N4–Cu2–O1	87.3(1)
O1–Cu1–O3	154.7(1)	N4–Cu2–O6	171.9(1)
O1–Cu1–O5	103.88(9)	N4–Cu2–O8	85.3(1)
C2–C1–C6	110.4(3)[a]		

[a] Average of the four corresponding angles is 110.4(6).

Table 5
Assignment of the $\nu(CO_2)_{as}$ and $\nu(CO_2)_s$ stretching frequencies for the solid complexes.

Complex	$\nu(CO_2)_{as}$ (cm^{-1})	$\nu(CO_2)_s$ (cm^{-1})
1	1619	1391
2	1625	1374
3	1612	1369, 1343
4	1627	1390, 1363
5	1626	1394, 1354

Table 6
Electrochemical data for $Cu(AA)_2$ complexes in DMF (the $E^{o\prime}_{1/2}$ of ferrocene was 490 ± 10 mV) at 100 mV/s scan rate.

Complex	$E^{o\prime}_{pa}$	$E^{o\prime}_{pc}$
1	−84	−659
2	−55	−692
3	−80	−754
4[*]	−80	−735
5	−63	−620

[*] Solubility of the complex was limited.

2.6. Synthesis of $[Cu^{II}(AIB)_2]$ (**4**)

Yield: 0.59 g (73%). *Anal.* Calc. for $C_8H_{16}CuN_2O_4$: C, 35.88; H, 6.02; N, 10.46. Found: C, 35.4; H, 6.1; N, 10.2. FT-IR bands (KBr pellet, cm^{-1}) 3273 (m), 3240 (m), 3142 (w), 2974 (m), 2933 (w), 1627 (vs), 1588 (m), 1474 (m), 1390 (s), 1363 (m), 1221 (s), 1097 (m), 1087 (m), 893 (w), 817 (w), 782 (m), 691 (w), 576 (w). UV–Vis (CH_3OH) [λ_{max}, nm ($\log\varepsilon$)] 244 (3.84), 600 (1.88).

2.7. Synthesis of $[Cu^{II}(D,L\text{-}ALA)_2]{\cdot}H_2O$ (**5**)

Yield: 0.58 g (81%). *Anal.* Calc. for $C_6H_{14}CuN_2O_3$: C, 27.96; H, 5.48; N, 10.87. Found: C, 28.2; H, 5.5; N, 11.0%. FT-IR bands (KBr

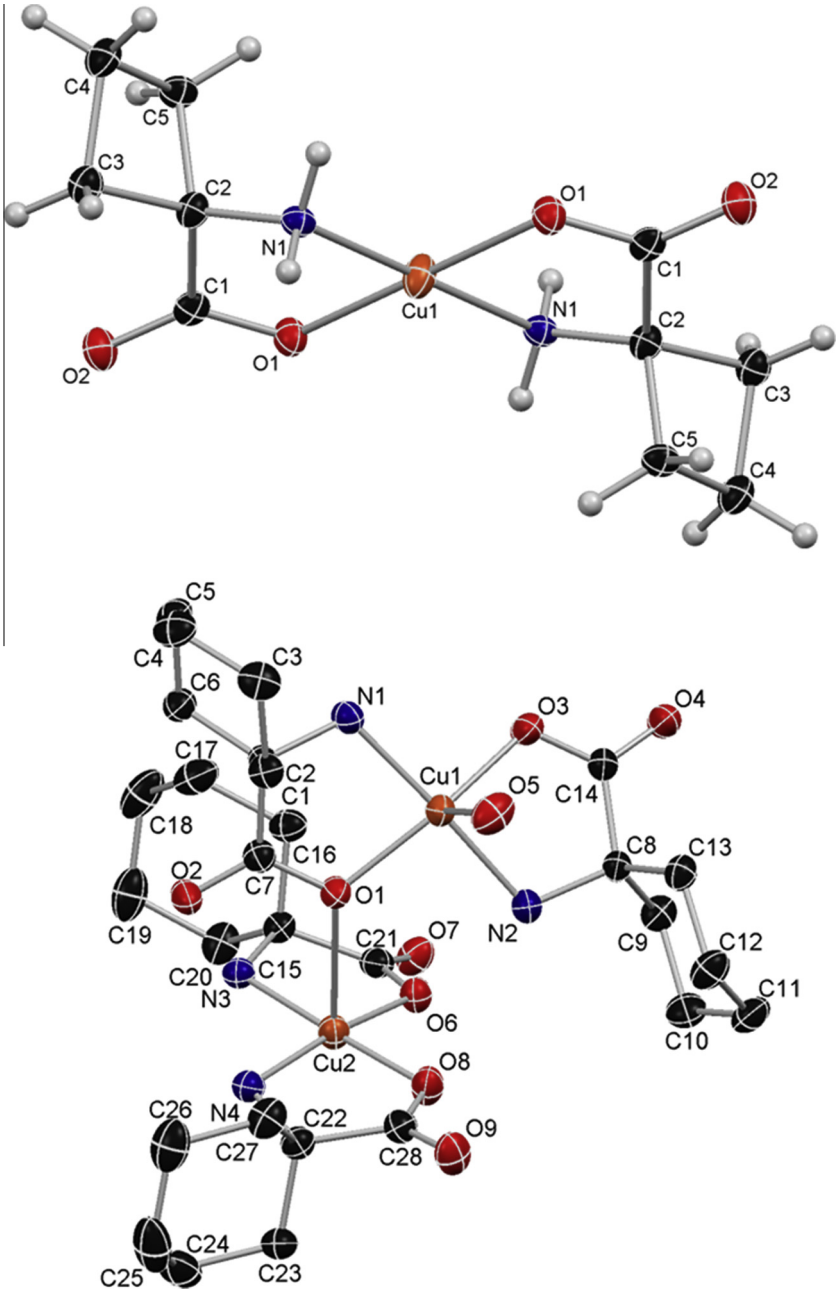

Fig. 1. X-ray structure of **1** and **3**. Ellipsoids are plotted at 30% probability level, hydrogen atoms are omitted for ACHC for clarity.

pellet, cm^{-1}) 3395 (m), 3267 (m), 3158 (w), 2970 (m), 2935 (w), 2877 (w), 1626 (vs), 1591 (s), 1451 (m), 1394 (s), 1354 (m), 1301 (m), 1160 (s), 1120 (s), 1062 (w), 857 (m), 789 (w), 672 (w), 566 (m). UV–Vis (CH_3OH/water) [λ_{max}, nm (log ε)] 239 (3.86), 610 (1.81).

2.8. Determination of products and kinetic measurements

Kinetic studies on the catalytic oxidation of amino acids by $CuCl_2$ or $Cu(AA)_2$ complexes were performed in a 3:1 DMF–water mixture at 35 °C. Assays were performed as follows: respective amino acid (3.6×10^{-4} mol) was dissolved in 10 mL of the solvent mixture in a sealable tube of 20 mL. To the mixture were then added MeCN (10 μL) as internal standard, the catalyst (7.2×10^{-8} mol) and NH_4OH (3.6×10^{-4} mol). Hydrogen peroxide (32 μL, 3.6×10^{-4} mol) was then added through the septum with a syringe and the evolved product(s) were measured by removing 250 μL of the headspace by GC analysis. The concentration of products in the head space are linearly proportional to the concentration of those in the reaction mixture.

3. Results and discussion

3.1. Synthesis and characterization of the complexes

The complexes were synthesized in methanol. Crystalline products were obtained by slow evaporation of the methanol from the reaction mixture. An overview of the isolated and characterized compounds is given in Table 1, crystal structure details for **1** and **3** are given in Table 2, the single crystal structures are shown in Fig. 1.

Selected bond lengths and angles are listed in Tables 3 and 4. The ligand geometry in **1** is *SP-4* and the ACBC ligands are located

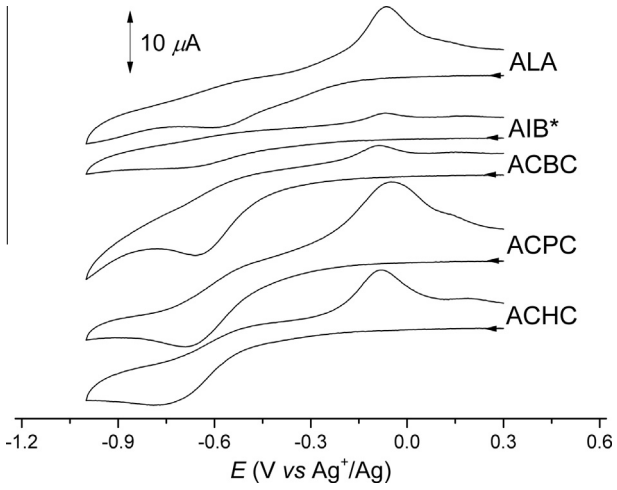

Fig. 2. Cyclic voltammograms of the AA complexes (DMF, 1 mM complex, 0.1 M TBAP electrolyte, at 100 mV/s scan rate).

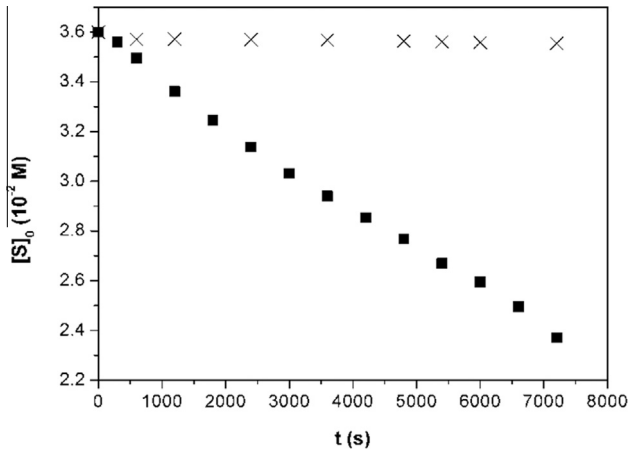

Fig. 3. Reaction of AIBH (■) and AIBH in the presence of AMEP (×) in DMF/water (3:1) at 35 °C. $[CuCl_2]_0 = 7.2 \times 10^{-6}$ M, $[AIBH]_0 = 3.6 \times 10^{-2}$ M, $[AMEPH]_0 = 0$ or 3.6×10^{-3} M, $[H_2O_2]_0 = 3.6 \times 10^{-2}$ M, $[NH_4OH]_0 = 3.6 \times 10^{-2}$ M.

in *trans*-arrangement. Thus the Cu(II) ions represent the inversion centre of the molecule and occupy face-centred positions of the centrosymmetric unit cell. The bond lengths are all below 2.0 Å. Remarkably the geometry lacks any distortions. Although the O2 atom of a neighboring complex is found 2.83 Å from Cu1 at the axial site, this contact is too long to be considered as a metal–ligand interaction. Weak H-bonds are listed in Fig. S1. In contrast, **3** is dinuclear with two different *SPY-5* sites. Regarding the equatorial planes, Cu1 is surrounded by two ACHC ligands in *trans*-, whereas Cu2 binds two ACHC ligands in *cis*-configuration. The O1 atom forms a bridge between Cu1 and Cu2, for the latter as an axial ligand. Finally, the axial site at Cu1 is occupied by a water molecule. The dimer is remarkably rich in H-bonds that are shown in Fig. S2. The τ values are somewhat different for the two sites (Table 3), yet both are best described as distorted square pyramidal. The configuration descriptors for the two centers are *SPY-5-21* for Cu1 and *SPY-5-12* for Cu2.

It is out of the scope of this study to consider the presumable role of the H-bonds and ring size of the amino acid R-group in the favored *trans*- vs. *cis*- arrangement of the ligands.

The IR spectral analysis of the solid complexes can be useful, since the characteristic $\nu(CO_2)_{as}$ and $\nu(CO_2)_s$ stretching frequencies for the carboxylate groups should be sensitive to coordination modes. According to the X-ray structures, between two Cu(II) centers a μ-carboxylato-κ*O*,κ*O'*-bridge exists in the solid state in **1** and **3**. The complexes exhibit relatively great difference between the $\nu(CO_2)_{as}$ and $\nu(CO_2)_s$ frequencies in the range 220–270 cm^{-1} that is in accordance with their bridging position (bands are listed

Table 7
Kinetic data for the oxidation of amino acids.[a]

Substrate	Product(s)	$CuCl_2$		$Cu(AA)_2$	
		$-d[S]/dt$ (10^{-7} Ms^{-})	TOF (h^{-1})	TOF (h^{-1})	BDE_{N-H}[b] (kcal/mol)
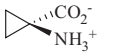 ACCH	ethylene	0.04	2	–	97.4
 ACBCH	cyclobutanone, dehydroproline, butyronitrile	2.40	103	166	–
 ACPCH	cyclopentanone	4.52	150	175	–
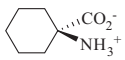 ACHCH	cyclohexanone	16.85	809	–	–
 ALAH	formaldehyde	2.20	9	14	98.8
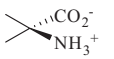 AIBH	acetone	19.60	853	860	100
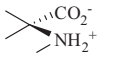 MAIBH	acetone	1.26	98	–	–

[a] In DMF/water (3:1) at 35 °C. $[CuCl_2]_0 = 7.2 \times 10^{-6}$ M, $[S]_0 = 3.6 \times 10^{-2}$ M, $[H_2O_2]_0 = 3.6 \times 10^{-2}$ M, $[NH_4OH]_0 = 3.6 \times 10^{-2}$ M.
[b] From Ref. [27].

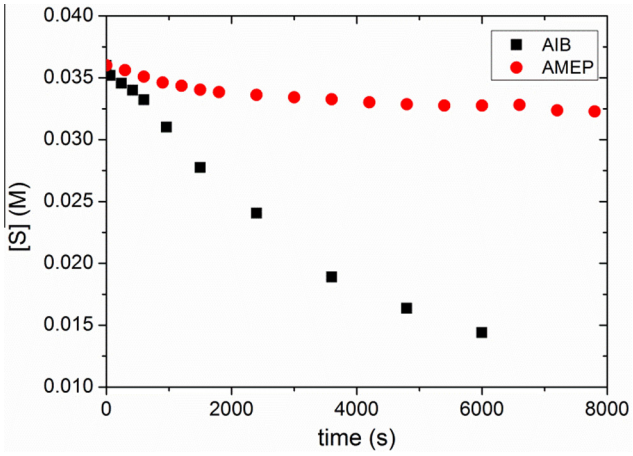

Fig. 4. Reaction of AIBH or AMEPH in DMF/water (3:1) at 35 °C. $[CuCl_2]_0 = 1.8 \times 10^{-3}$ M, $[AIBH]_0$ (or $[AMEPH]_0$) = 3.6×10^{-2} M, $[H_2O_2]_0 = 3.6 \times 10^{-2}$ M, $[NH_4OH]_0 = 3.6 \times 10^{-2}$ M.

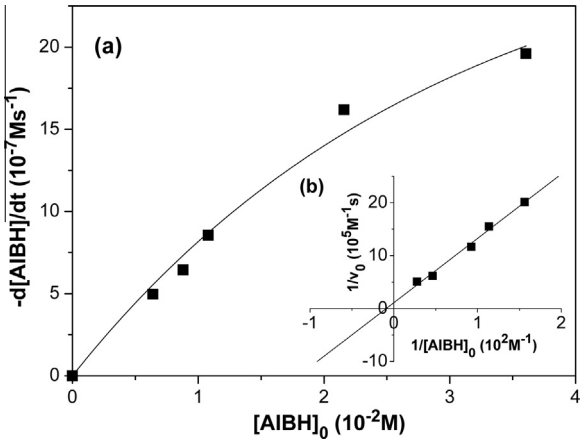

Fig. 5. (a) Changes in the rate of the reaction of AIBH with the initial substrate concentration in DMF/water (3: 1) at 35 °C, $[CuCl_2]_0 = 7.2 \times 10^{-6}$ M, $[H_2O_2]_0 = 3.6 \times 10^{-2}$ M, $[NH_4OH]_0 = 3.6 \times 10^{-2}$ M; (b) Lineweaver–Burk plot. (For data see Table S1).

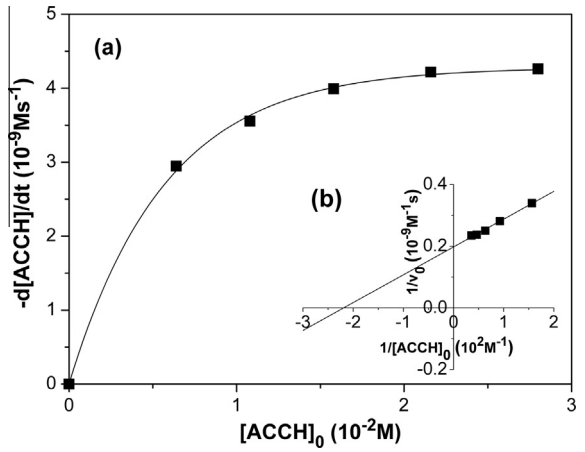

Fig. 6. (a) Changes in the rate of the reaction of ACCH with the initial substrate concentration in DMF/water (3: 1) at 35 °C, $[CuCl_2]_0 = 7.2 \times 10^{-6}$ M, $[H_2O_2]_0 = 3.6 \times 10^{-2}$ M, $[NH_4OH]_0 = 3.6 \times 10^{-2}$ M (b) Lineweaver–Burk plot. (For data see Table S2).

Table 8
Kinetic data for the oxidation of AIBH and ACCH by $CuCl_2$ in DMF/water (3:1).

	AIBH	ACCH
k_{cat} (s^{-1})	1.25	0.0007
K_M (mM)	110	4.5
SIE	3.14	1.44

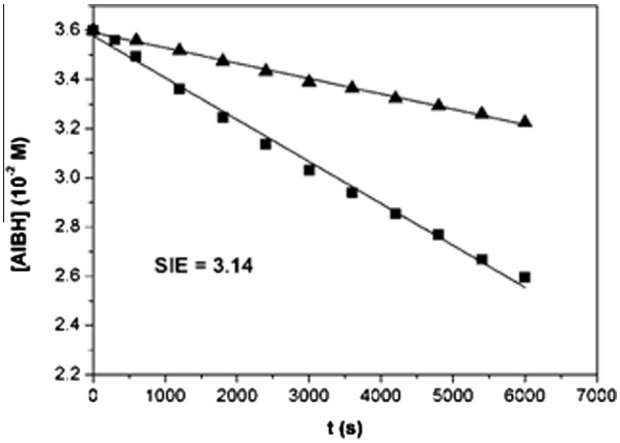

Fig. 7. Progress of the oxidation reaction of AIBH in DMF/water (■) and DMF/deuterium-oxide (▲) (3:1) at 35 °C. [AIBH] = 3.6×10^{-2} M, $[CuCl_2] = 7.2 \times 10^{-6}$ M, $[NH_4OH] = 3.6 \times 10^{-2}$ M.

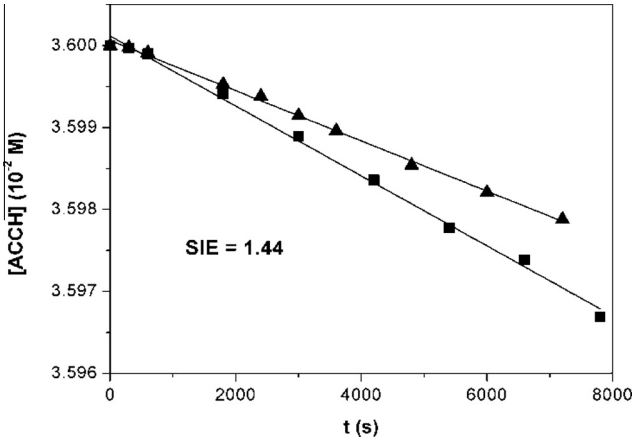

Fig. 8. Progress of the oxidation reaction of ACCH in DMF/water (■) and DMF/deuterium-oxide (▲) (3:1) at 35 °C. [ACCH] = 3.6×10^{-2} M, $[CuCl_2] = 7.2 \times 10^{-6}$ M, $[NH_4OH] = 3.6 \times 10^{-2}$ M.

in Table 5). However, without isotope labeling the assignment of the $\nu(CO_2)_s$ stretching for the $[Cu(AA)_2]$ complexes can be ambiguous due to the presence of two bands in the concerned 1400–1300 cm^{-1} region. Nevertheless, considering the lowest possible $\nu(CO_2)_s$, the $\nu(CO_2)_{as}$–$\nu(CO_2)_s$ difference is still >200 cm^{-1} in each spectrum. The multiple frequencies of symmetric stretching modes may originate from the different binding positions for the carboxylates in structures similar or identical to that of **3**.

3.2. Redox properties of $Cu(AA)_2$ (**1–5**) complexes

The electrochemical properties of the $Cu(AA)_2$ complexes **1–5** were studied by cyclic voltammetry (CV) to the cathodic direction, in DMF, at room temperature under argon. The CV curves are

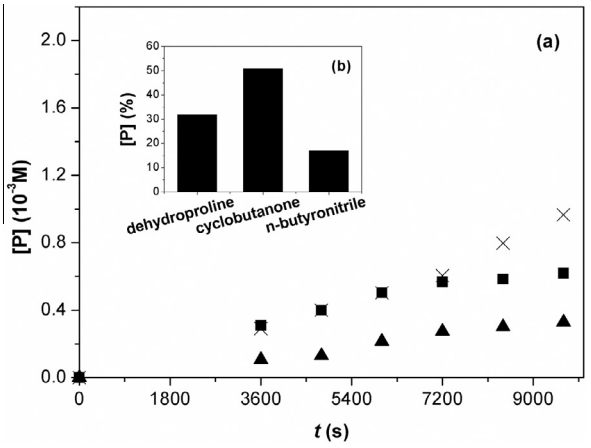

Fig. 9. (a) Progress of the oxidation reaction of ACBH in DMF/water (3:1) at 35 °C. [ACBCH] = 3.6×10^{-2} M, [$CuCl_2$] = 7.2×10^{-6} M, [H_2O_2]$_0$ = 3.6×10^{-2} M, [NH_4OH]$_0$ = 3.6×10^{-2} M. Cyclobutanone (×), dehydroproline (■), *n*-butyronitrile (▲), (b) Proportion of the products.

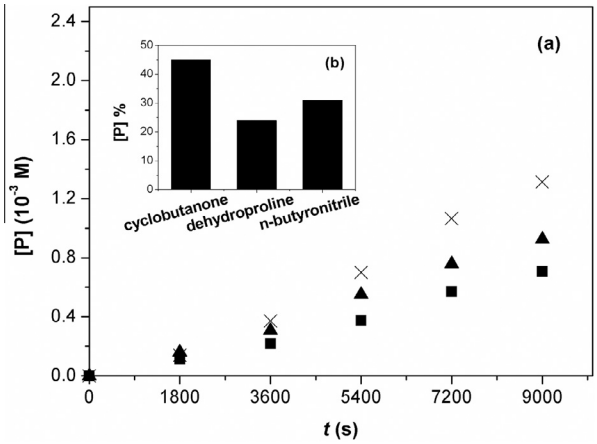

Fig. 10. (a) Progress of the oxidation reaction of $Cu^{II}(ACBC)_2$ (**6**) in DMF/water (3:1) at 35 °C. [$Cu^{II}(ACB)_2$] = 3.6×10^{-2} M, [H_2O_2]$_0$ = 3.6×10^{-2} M, [NH_4OH]$_0$ = 3.6×10^{-2} M. Cyclobutanone (×), dehydroproline (■), *n*-butyronitrile (▲), (b) Proportion of the products.

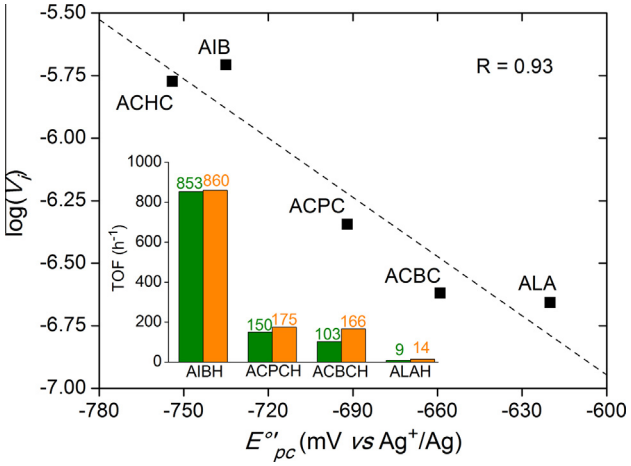

Fig. 11. The log(V_i) values as a function of $E^{\circ\prime}_{pc}$ of the corresponding $Cu(AA)_2$ complexes. Insert: TOF values with $CuCl_2$ (green) or $Cu(AA)_2$ (orange) as catalyst among identical conditions. Data are listed in Tables 6 and 7, log(Vi) values in this figure are identical to the logarithm of corresponding −d[S]/dt values in Table 7. (Colour online.)

shown in Fig. 2 and the observed peak potentials are listed in Table 6. The CVs all show one irreversible cathodic reduction peak that varies with the AAs (between −620 and −754 mV), except for the alanine complex that exhibits a pre-peak shoulder, too. The irreversibility may be associated with a geometric change in the coordination sphere to achieve stabilization from square planar for Cu(II) to tetrahedral for Cu(I) as supported by DFT calculations that have previously been carried out on similar Cu-AA complexes [26], or other changes in the ligand environment induced by the gained negative charge. Whichever is the case, the reverse scan to the anodic direction yields a peak that is non-Nernstian in its profile suggestive of an ECE mechanism that necessarily precludes any type of further straightforward analysis at this level.

3.3. Catalysis

Toward an efficient catalytic system we first started studies using directly $CuCl_2$ as catalyst in DMF/H_2O (3:1) mixtures at 35 °C with 1:5000:5000 [Cu]:[substrate]:[H_2O_2] ratios and by adding 5000 equivalents of ammonium hydroxide as base. The results from the experiments are summarized in Table 7. The highest TOF values were observed with ACHCH among the cyclic and AIBH among acyclic substrates. It is remarkable that the *N*-methyl group in MAIBH causes roughly an order of magnitude decrease in the reaction rate.

When AMEPH is present in the catalytic system (500 equivalents is added to the 1:5000:5000 Cu:AIBH:H_2O_2 mixture) the reaction is completely inhibited and no acetone can be detected (Fig. 3). However, if we made an experiment with an increased copper concentration (250:5000:5000) and only AMEPH present, the conversion of AMEPH to acetone was 12% corresponding to a TON of 2.4. In comparison, AIBH is converted by 60% to acetone among the same conditions, corresponding to a TON of 12 (see Fig. 4 for more details). Moreover, pseudo-first-order rate constants could be obtained for both reactions: $k'_{AIBH} = (1.60 \pm 0.05) \times 10^{-4}\ s^{-1}$ and $k'_{AMEPH} = (0.35 \pm 0.02) \times 10^{-4}\ s^{-1}$. These give a $k'_{AIBH}/k'_{AMEPH} = k_{rel}$ of 4.6, a significant lowering in reaction rate that fits well the ratio of the corresponding TON's. These results explain the inhibition of the AIBH oxidation when AMEPH is present.

In two cases (ACCH and AIBH) the substrate dependence was also investigated. The saturation kinetics (Figs. 5 and 6) suggest a pre-equilibrium between the substrate and the catalyst. From the Lineweaver–Burk plots the K_M and k_{cat} parameters could be determined (Table 8). These are in accordance with the much higher reactivity of the AIBH than ACCH as experienced with **5** and **1** and similarly in the Fe-based catalytic systems [8].

The BDE values for the N–H bonds of the amino acids are very similar and do not correlate with the reactivity order (Table 7). SIE's were investigated for AIBH and ACCH and the low values (Figs. 7 and 8, Table 8) are in the range typical for an ET-PT mechanism. It seems likely that the formation of the imine radical (the generally assumed initiating step of the ACCO reaction) from the coordinated, anionic amino acids, takes place via an ET-PT mechanism.

ACBCH deserves more detailed discussion as this substrate is unique considering its dual degradation pathway. Three products were observed during catalysis (Figs. 9 and 10): dehydroproline and *n*-butyronitrile (according to pathway **C** in Scheme 1), and cyclobutanone (according to pathway **B** in Scheme 1). While the latter is analogous to the degradation of AIBH and cyclic AAs with $n > 2$ the former products correspond to the ACCH degradation. It can be said that the major product is cyclobutanone in both cases with similar proportion. In all other cases the reactions selectively provided the ketone products.

Since $Cu(AA)_2$ complexes are well known it seemed reasonable that during the catalysis such *bis*-chelate complexes may occur. To check this possibility we used the synthesized $Cu(AA)_2$ complexes including our new *bis*(1-amino(cyclo)alkane-1-carboxylato-κ^2N,O)copper(II)

complexes as catalysts and determined the TOF values for the reactions with **1**, **2**, **4** and **5** (Table 7). Only minimal differences between the TOFs of runs conducted with $Cu(AA)_2$ and $CuCl_2$ were found (Fig. 11 insert) indicating that the dominant form of the catalyst may be the same. Moreover, when the logarithm of the initial rate of the reactions (based on product analysis) is plotted against the $E^{\circ\prime}_{pc}$ of the $Cu(AA)_2$ complexes a correlation with negative slope can be obtained (Fig. 11). On thermodynamic grounds this allows the conclusion that among the various amino acids those will be oxidized the most efficiently by hydrogen peroxide, which are the stronger reducing agents in their Cu(I) form.

4. Conclusion

Catalytic systems using Cu(II) were first tested as ACCO models. Trends in the Cu(II) to Cu(I) reduction potentials from cyclic voltammetry and the rates of the amino acid oxidations imply identical initial step for the peroxide/copper activation that is followed by the formation of the various products. It is assumable that simple $Cu(AA)_2$ complexes (two of which have been structurally characterized) accelerate AA decomposition if peroxide is present even with $CuCl_2$ precursor. Our results raise the question how much Cu(II) ions bound in oxidase and oxygenase enzymes (where peroxide may be generated at the active site) can contribute to protein degradation *in vivo*?

Acknowledgments

Financial support of the Hungarian National Research Fund (OTKA K108489), TÁMOP-4.2.2.A-11/1/KONV-2012-0071, TÁMOP 4.2.4.A/2-11-1-2012-0001 (S. Góger), TÁMOP-4.2.2/B-10/1-2010-0025, and COST CM1003 is greatfully acknowedged. This project was also supported by the János Bolyai Scolarship of the Hungarian Academy of Sciences (J. S. Pap).

Appendix A. Supplementary data

CCDC 941371 and 941372 contains the supplementary crystallographic data for **1** and **2**. These data can be obtained free of charge via http://www.ccdc.cam.ac.uk/conts/retrieving.html, or from the Cambridge Crystallographic Data Centre, 12 Union Road, Cambridge CB2 1EZ, UK; fax: (+44) 1223-336-033; or e-mail: deposit@ccdc.cam.ac.uk. Supplementary data associated with this article can be found, in the online version, at http://dx.doi.org/10.1016/j.poly.2014.02.007.

References

[1] M.L. Trehy, R.A. Yost, C.J. Miles, Environ. Sci. Technol. 20 (1986) 1117.
[2] L. Padhye, U. Tezel, W.A. Mitch, S. Pavlostathis, C.-H. Huang, Environ. Sci. Technol. 43 (2009) 3087.
[3] N. Noorhasan, B. Patel, V.K. Sharma, Water Res. 44 (2010) 927.
[4] K.S. Rangappa, K. Manjunatha Swamy, M.P. Raghavendra, N.M.M. Gowda, Int. J. Chem. Kinet. 34 (2002) 49.
[5] S.D. Quine, B.T. Gowda, Oxidation Commun. 21 (1998) 106.
[6] P.A. Prasantha, N.C. Sandhya, B.K. Kempegowda, D.G. Bhadregowda, K. Mantelingu, S. Ananda, K.K.S. Rangappa, M.N. Kumara, J. Mol. Catal. A: Chem. 353–354 (2012) 111.
[7] G. Baráth, J. Kaizer, J.S. Pap, G. Speier, N. El Bakkali-Taheri, A.J. Simaan, J. Chem. Commun. 46 (2010) 7391.
[8] S. Góger, D. Bogáth, G. Baráth, A.J. Simaan, G. Speier, J. Kaizer, J. Inorg. Biochem. 123 (2013) 46.
[9] L. Brisson, N. El Bakkali-Taheri, M. Giorgi, A. Fadel, J. Kaizer, M. Réglier, T. Tron, E.H. Ajandouz, A.J. Simaan, J. Biol. Inorg. Chem. 17 (2012) 939.
[10] D.E. Richardson, C.A. Regino, H. Yao, J.V. Johnson, Free Radical Biol. Med. 35 (2003) 1538.
[11] R. Rafael, A. Beatriz, F.S. Gerardo, A.F. Bruce, Free Radical Biol. Med. 25 (1998) S65.
[12] G.P. Panigrahi, R.C. Paichha, Int. J. Chem. Kinet. 23 (1990) 345.
[13] Y. Zelechonok, R.B. Silverman, J. Org. Chem. 57 (1992) 5787.
[14] M.S. Ramachandran, T.S. Vivekanandam, J. Chem. Soc., Perkin Trans. II (1984) 1341.
[15] M.S. Ramachandran, T.S. Vivekanandam, R.P.M. Raj, J. Chem. Soc., Perkin Trans. II (1984) 1345.
[16] M.S. Ramachandran, T.S. Vivekanandam, Tetrahedron 40 (1984) 4929.
[17] S.K. Rani, D. Easwaramoorthy, I.M. Bilal, M. Palanichamy, Appl. Catal. A: Gen. 369 (2009) 1.
[18] E.R. Stadtmann, R.L. Levine, Amino Acids 25 (2003) 207.
[19] B.S. Berlett, E.R. Stadtman, J. Biol. Chem. 272 (1997) 20313.
[20] K.C. Brown, S.-H. Yang, T. Kodadek, Biochemistry 34 (1995) 4733.
[21] B. Cuenoud, T.M. Tarasow, A. Schepartz, Tetrahedron Lett. 33 (1992) 895.
[22] A.I. Bush, Curr. Opin. Chem. Biol. 4 (2000) 184.
[23] S. Varadarajan, S. Yatin, M. Aksenova, D.A. Butterfield, J. Struct. Biol. 130 (2000) 184.
[24] D.D. Perrin, W.L. Armarego, D.R. Perrin, Purification of Laboratory Chemicals, second ed., Pergamon Press, New York, 1990.
[25] G.M. Sheldrick, Acta Crystallogr., Sect. A 64 (2008) 112.
[26] W. Ghattas, M. Giorgi, Y. Mekmouche, T. Tanaka, A. Rockenbauer, M. Reglier, Y. Hitomi, A.J. Simaan, Inorg. Chem. 47 (2008) 4627.
[27] J. Thrower, L.M. Mirica, K.P. McCusker, J.P. Klinman, Biochemistry 45 (2006) 13108.